4. Improvement of Crystal and Optical Properties by $Al_{0.06}Ga_{0.94}N$/GaN SLS Underlayer

This chapter reports enhanced internal quantum efficiency (η_{iqe}) in InGaN-based multi-quantum well (MQW) grown on Si(111) substrate with $Al_{0.06}Ga_{0.94}N$/GaN strained-layer superlattice (SLS) cladding underlayer for application in light emitting devices.

In section 4.1, a comparative study between a thick $Al_{0.03}Ga_{0.97}N$ bulk and an $Al_{0.06}Ga_{0.94}N$/GaN SLS cladding layer is performed. Transmission electron microscopy (TEM) images reveal that $Al_{0.06}Ga_{0.94}N$/GaN SLS cladding underlayer is effective to suppress threading dislocations (TDs). A higher η_{iqe} has been achieved in sample with $Al_{0.06}Ga_{0.94}N$/GaN SLS cladding underlayer, compared to that of $Al_{0.03}Ga_{0.97}N$ bulk cladding layer. Internal quantum efficiency (η_{iqe}) of 31.6% has been achieved in sample with $Al_{0.06}Ga_{0.94}N$/GaN SLS cladding underlayer when the MQW thickness is reduced to 2 nm.

In section 4.2, a more detailed study has been performed on sample with $Al_{0.06}Ga_{0.94}N$/GaN SLS cladding underlayer, relative to conventional sample with GaN underlayer. The $Al_{0.06}Ga_{0.94}N$/GaN SLS underlayer improves emission wavelength uniformity and shows a narrower emission full-width at half-maximum (FWHM) than that of conventional GaN underlayer. A Gaussian fitting was performed to photoluminescence (PL) spectra to obtain emission wavelength behavior and integrated intensity of the peak energy. A higher MQW η_{iqe} of 29.4% is obtained in sample with $Al_{0.06}Ga_{0.94}N$/GaN SLS underlayer than that of 20.6% in GaN underlayer. TEM analysis

indicates that the $Al_{0.06}Ga_{0.94}N$/GaN SLS layer abruptly bends TD lines thus reduces threading dislocation density (TDD) to the MQW. Reciprocal space mapping (RSM) suggests that compressive strain in the GaN portion of $Al_{0.06}Ga_{0.94}N$/GaN SLS forces the abrupt inclination of the threading dislocations.

In section 4.3, a study is performed on growth and material characterization of InGaN-based laser diode (LD) structure grown on Si(111) substrate with a high-temperature grown thin AlN buffer layer and AlN/GaN multilayer (ML) intermediate layers. Two types of LD structures on Si(111) were prepared, (a) with bulk n- and p-type AlGaN cladding layer, and (b) with SLS n- and p-type AlGaN/GaN cladding layer. Active layer with 3 periods of $In_{0.10}Ga_{0.90}N/In_{0.03}Ga_{0.97}N$ MQW is sandwiched between the cladding layers. A standard LD structure with identical MQW parameter grown on GaN(0001) free-standing substrate was also prepared for comparison. Mirror-like and meltback-etching free surfaces have been achieved for both of the samples grown on Si(111) substrate. High-resolution x-ray diffraction (HRXRD) ω-2θ scan and scanning transmission electron microscopy (STEM) cross-sectional images reveal that a good quality of MQW with abrupt interfaces have been achieved for both of the samples grown on Si(111) substrate. Temperature-dependent PL measurement reveals that LD structure grown on Si(111) with SLS cladding layer has higher η_{iqe} than that of the sample with bulk cladding layer.

4.1 Comparative Study of $Al_{0.06}Ga_{0.94}N$/GaN SLS Underlayer and $Al_{0.03}GA_{0.97}N$ Bulk Cladding Underlayer

4.1.1 Introduction

GaN-based wide band-gap emitters grown on Si are very promising breakthrough for low-cost energy-saving applications. Si is a very promising substrate for GaN growth, because of its low cost, wide availability, large surface diameter, and offering good current and thermal conductivity for device operation. However, a few issues that hindered epitaxial-growth of GaN on Si(111) substrate are cloudy and cracked epilayer, large wafer curvature and high TDD exceeding 10^{10} cm^{-2} in conventional metal organic chemical vapor deposition (MOCVD) method. These are attributed by large lattice and thermal mismatch between GaN epilayer and Si(111) substrate of 17% and 116%, respectively. A thin AlN layer is generally used as seeding layer for GaN growth on Si substrate, followed by methods such as AlN/GaN or AlGaN/GaN multilayer [1-5], AlN interlayer [6-7], Si_xN_{1-x} interlayer [8-9], etc, to offset tensile and thermal stress between GaN and Si, and to improve crystal quality in the subsequent epilayer.

Despite the difficulties for GaN growth on Si, several groups have succeeded in growing good epitaxial quality GaN layer on Si(111) substrate with applications in light emitting diode (LED) [2-5] and high electron mobility transistor (HEMT) [10]. In this section, the author reports an efficient suppression of TDs in InGaN-based MQW sample grown on Si(111) substrate by an underlying $Al_{0.06}Ga_{0.94}N$/GaN SLS cladding layer, and an improvement of MQW η_{iqe} by optimizing MQW thickness in sample with

underlying $Al_{0.06}Ga_{0.94}N$/GaN SLS cladding layer. This work is intended for applications in GaN-based LD and LED grown on Si substrate.

4.1.2 Experimental Methods

Samples in this study were grown on 2 inches Si(111) substrate by horizontal-reactor MOCVD. Trimethylgallium (TMGa), trimethylaluminum (TMAl) and ammonia (NH_3) were used as precursors for Ga, Al and N, respectively. Hydrogen (H_2) was used as carrier gas. Monosilane (SiH_4) diluted in hydrogen was used for n-type dopant. Prior to growth, the substrate was thermally cleaned at 1100 °C in H_2 flow. A 20 nm thin AlN layer was grown on the Si(111) substrate as seeding layer, followed by 40 pairs of AlN/GaN ML with respective thickness of 5 nm and 20 nm. Two types of cladding layer were grown on the ML, (a) with a thick $Al_{0.03}Ga_{0.97}N$ bulk layer, and (b) with SLS layer consisting of $Al_{0.06}Ga_{0.94}N$/GaN pairs. Subsequently, a 60 nm GaN waveguide layer and an active layer, with 3 pairs of 4 nm $In_{0.16}Ga_{0.84}N$ quantum wells and 9 nm of Si-doped $In_{0.08}Ga_{0.92}N$ barriers were grown. Finally, the growth was capped with a 10 nm GaN layer. Furthermore, optical characteristics in sample with underlying $Al_{0.06}Ga_{0.94}N$/GaN SLS cladding layer was optimized by reducing the MQW thickness to 3 nm and 2 nm. MQW pairs and other growth parameters were kept similar in all samples.

Structural properties were evaluated by TEM, observed using JEOL JEM-2010F FasTEM system operating at 200 kV. TEM samples were prepared by a standard procedure, with thickness of 100 nm. Optical characteristics were evaluated by temperature-dependent PL method, using a pulse tube helium cryostat (Iwatani Cryo

Mini) equipped with heater and temperature controller. A 325 nm He-Cd laser was used for PL excitation.

4.1.3 Results and Discussions

All samples in this study are crack-free, having specular surface and free from meltback-etching. TEM cross-sectional bright-field images of the samples are shown in Fig. 4.1, with sample of $Al_{0.03}Ga_{0.97}N$ bulk cladding layer shown in (a) and (b), and sample of $Al_{0.06}Ga_{0.94}N$/GaN SLS cladding layer shown in (c) and (d). Major layers are marked in the figures. The TEM images are taken with $\boldsymbol{g}=[0002]$ and $\boldsymbol{g}=[11\bar{2}0]$ diffraction conditions, making screw dislocation with $\boldsymbol{b}=[0001]$ and edge dislocation with $\boldsymbol{b}=(1/3)[11\bar{2}0]$ visible in respective diffraction. Mixed dislocation with $\boldsymbol{b}=(1/3)[11\bar{2}3]$ can be observed in both planes, according to the $\boldsymbol{g}\times\boldsymbol{b}$ invisibility criterion.

A high density of TDs consisting of stacking faults, fault loops and coalescing dislocations can be observed originating at the AlN seeding layer, which is attributed by large lattice and thermal mismatch with the Si(111) substrate. However, TDs are bent and reduced as the AlN/GaN ML pair is increased. TDs which penetrate to the upper edge of the ML surpass the interface and further penetrate into the cladding layer. In sample with thick $Al_{0.03}Ga_{0.97}N$ bulk cladding layer, formation of new dislocations can also be observed at the interface due to sudden change of lattice constant between AlN/GaN ML and $Al_{0.03}Ga_{0.97}N$ cladding layer. TDs at the lower edge in the $Al_{0.03}Ga_{0.97}N$ cladding layer bend, and several TDs intersect into another single TD propagating vertically towards sample surface which is normally seen in a thick relaxed

GaN-based layer.

In contrast to that phenomenon, in sample with $Al_{0.06}Ga_{0.94}N$/GaN SLS cladding layer, TDs surpassing the interface between AlN/GaN ML and $Al_{0.06}Ga_{0.94}N$/GaN radically disappear at the lower region in the $Al_{0.06}Ga_{0.94}N$/GaN SLS cladding layer. Interestingly, we do not observe any formation of new TD at the interface. TDs that surpass the interface bend abruptly and annihilate in the $Al_{0.06}Ga_{0.94}N$/GaN SLS cladding layer. The initial pair of $Al_{0.06}Ga_{0.94}N$/GaN SLS cladding layer is compressive to resemble lattice constants of the underlying AlN/GaN ML. This behavior can prevent formation of new TD at the interface. The SLS gradually returns to its stable strain state as the SLS pair number is increased. The existence of strain between $Al_{0.06}Ga_{0.94}N$ and GaN layer in the SLS pair is proposed to force TDs to bend at abrupt angle and annihilate in the cladding layer.

TDD in the upper region of each cladding layer is summarized in Table IV.I. The TDD estimation was determined by counting along crystal plane normal to the growth direction from TEM micrograph of 5 μm length and 100 nm sample thickness. Edge and mixed type of dislocations are predominant in both samples. We find that TDD of screw and mixed type at $\boldsymbol{g}=[0002]$, and edge and mixed type at $\boldsymbol{g}=[11\bar{2}0]$ in sample with $Al_{0.06}Ga_{0.94}N$/GaN SLS cladding layer is reduced compared to that of sample with thick $Al_{0.03}Ga_{0.97}N$ bulk cladding layer. This confirms that SLS cladding layer is effective to annihilate TDs in GaN-based hetero-epitaxy on Si(111) substrate.

MQW optical performance in each underlying cladding layer was evaluated by temperature-dependent PL. Fig. 4.2 shows Arrhenius plot of normalized integrated intensity for the MQW emission with 10 K temperature increment between 10 and 100 K, and 20 K increment subsequently until 300 K. The MQW η_{iqe} can be estimated by

comparing PL normalized integrated intensity ratio at 300 K and 10 K [11]. Assuming η_{iqe} at 10 K is 100%, estimation of η_{iqe} at 300 K for sample with identical 4 nm MQW thickness are 2.1% and 4.8% in sample with underlying $Al_{0.03}Ga_{0.97}N$ bulk and $Al_{0.06}Ga_{0.94}N$/GaN SLS, respectively. The enhancement of η_{iqe} is attributed by efficient suppression of TDs by the SLS cladding layer, as discussed earlier.

Further improvement of the η_{iqe} can be achieved by reducing the MQW layer thickness, which reduces quantum-confined Stark effect (QCSE) and increases electron-hole wave-function overlap in the InGaN-based MQWs [12]. Sample with 3 and 2 nm MQW thicknesses show respective estimated η_{iqe} of 11.2% and 31.6%, when grown with underlying $Al_{0.06}Ga_{0.94}N$/GaN SLS cladding layer. The steep decrease of integrated intensity in temperature range between 120 K and 160 K is attributed by activation of non-radiative process in the recombination [13].

Fig. 4.3 shows temperature-dependent normalized PL intensity for sample with 2 nm thickness of $In_xGa_{1-x}N$ MQW grown with underlying $Al_{0.06}Ga_{0.94}N$/GaN SLS cladding layer. The emission at 2.9 eV originates from radiative recombination of excitons in the wells, while emission at 3.1 eV which is visible at low temperature originates from $In_yGa_{1-y}N$ barriers. The intensity ratio at 300 K and 10 K is consistent with the estimated η_{iqe} in Fig. 4.2. These results confirm that $Al_{0.06}Ga_{0.94}N$/GaN SLS cladding layer is effective to suppress TDs and therefore enhance optical emission in InGaN-based MQW grown on Si(111) substrate with a relatively low pair numbers of MQW.

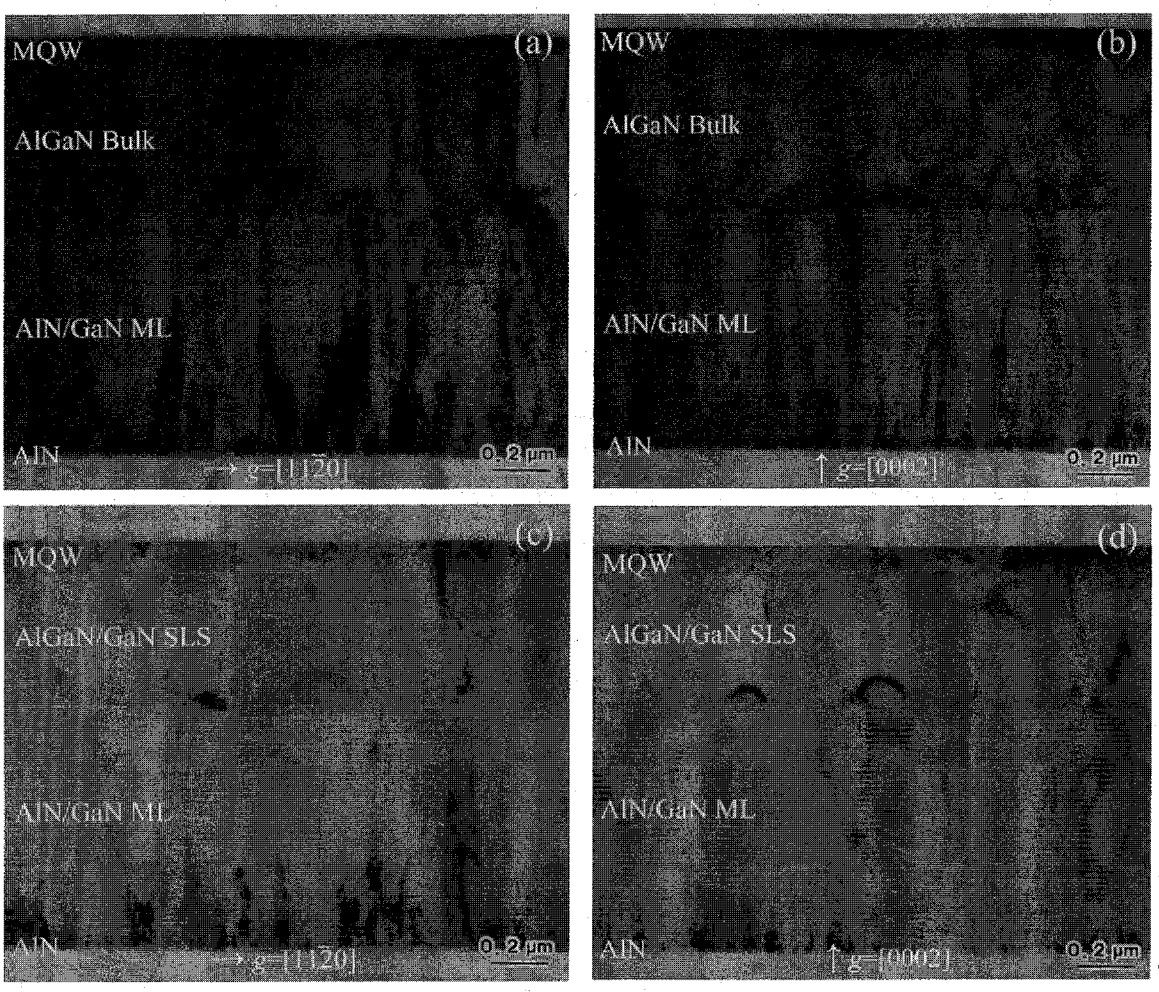

Fig. 4.1. TEM cross-sectional bright-field images of epitaxial structure on Si(111) substrate in this study. Sample with $Al_{0.03}Ga_{0.97}N$ bulk cladding layer is shown in (a) and (b), while sample with $Al_{0.06}Ga_{0.94}N$/GaN SLS cladding layer is shown in (c) and (d). Diffraction plane is marked in each figure.

Table IV.I. TDD in the upper region of each type of cladding layer determined from TEM micrograph.

Type of Cladding Layer	Threading Dislocation Density (cm^{-2})	
	Screw and Mixed $\boldsymbol{g}=[0002]$	Edge and Mixed $\boldsymbol{g}=[11\bar{2}0]$
$Al_{0.03}Ga_{0.97}N$ Bulk	8.4×10^{9}	1.5×10^{10}
$Al_{0.06}Ga_{0.94}N$/GaN SLS	3.4×10^{9}	6.5×10^{9}

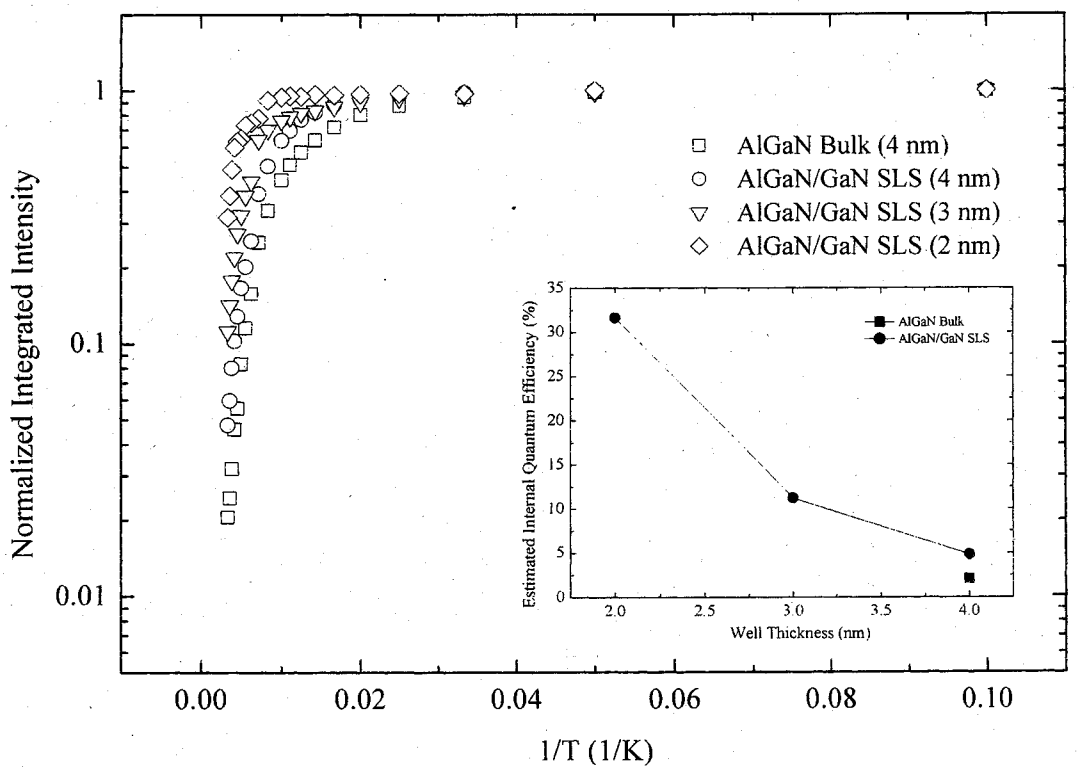

Fig 4.2. Normalized temperature-dependent PL integrated intensity for $Al_{0.03}Ga_{0.97}N$ bulk cladding layer and $Al_{0.06}Ga_{0.94}N$/GaN SLS cladding layer. Inset: Estimated PL η_{iqe} as a function of well thickness.

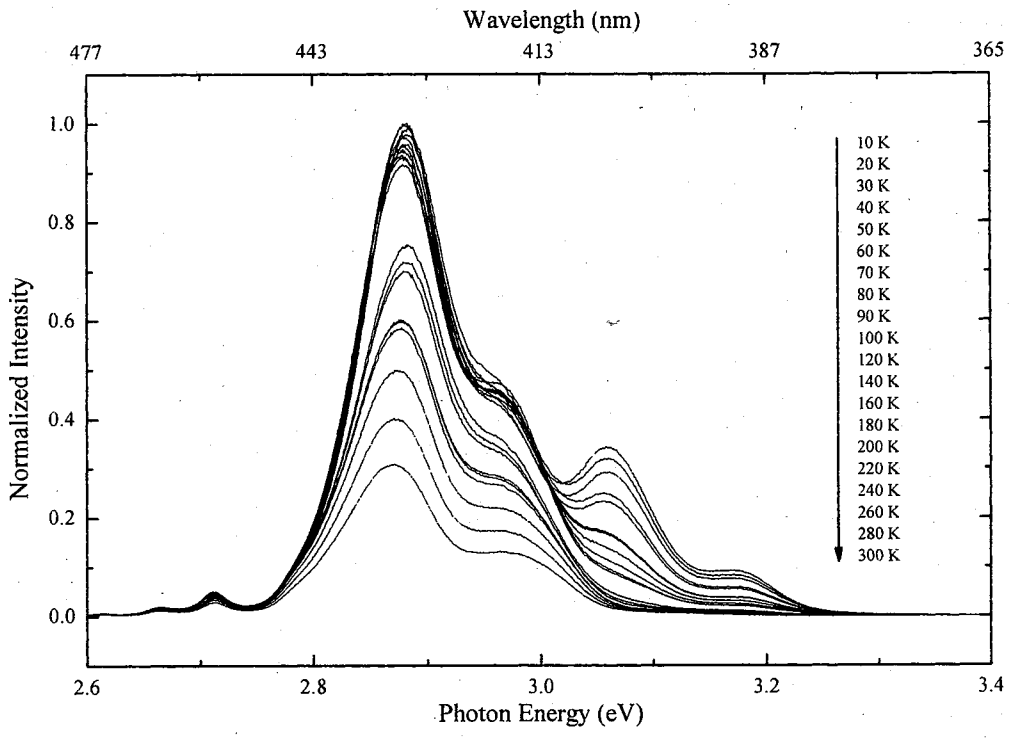

Fig. 4.3. Normalized temperature-dependent PL intensity for 3 pairs of 2 nm thickness InGaN-based MQW grown with underlying $Al_{0.06}Ga_{0.94}N$/GaN SLS cladding layer on Si(111) substrate.

4.2 Comparative Study of $Al_{0.06}Ga_{0.94}N$/GaN SLS Cladding Underlayer and GaN Underlayer

4.2.1 Introduction

Si(111) is a very promising substrate for GaN hetero-epitaxial growth which offers good current and thermal conductivity, large surface diameter, wide availability, and relatively cheaper than any other conventional substrates for nitride growth such as Al_2O_3 (sapphire) or SiC. Despite of the advantages, growth of GaN on Si substrate is more complicated due to the large lattice and thermal mismatch between GaN epilayer and Si(111) substrate of 17% and 116%, respectively. These factors attribute to large wafer bending, epilayer with high TDD ($\sim 10^{10}$ cm^{-2}) and cracks to relax the large tensile stress induced by the substrate [14]. Narrower band-gap width of the Si substrate is also absorptive to InGaN-based MQW emission [15].

Several groups have successfully achieved a good quality GaN hetero-epitaxial growth on Si(111) substrate grown by horizontal-reactor MOCVD using a thin AlN nucleation layer [14-19]. A stack of intermediate layers like AlN/GaN or $Al_xGa_{1-x}N$/GaN multilayer [14-17], AlN interlayer [18], Si_xN_{1-x} interlayer [19], etc, are used to offset the lattice and thermal stress, and further improve crystal quality in the subsequent GaN layer. InGaN-based blue LED grown with distributed Bragg reflector (DBR) was reported by Ishikawa *et al.* to reduce light absorption by the Si(111) substrate [15]. However, the DBR pair number is limited to obtain a crack-free layer. Moreover, DBR with high Al composition is disruptive to current propagation in vertical device structure on Si(111) substrate. No further report on TDs and η_{iqe} has been made so far for the

DBR structure.

In this section. the author reports effect of the insertion of $Al_{0.06}Ga_{0.94}N$/GaN SLS cladding underlayer to InGaN-based MQW structure grown on Si(111) substrate with AlN/GaN ML intermediate layer. SLS cladding layer is used instead of DBR layer for its superiority in vertical carrier propagation by tunneling-effect while simultaneously maintains good reflectivity. Reflectivity can also be improved by adding more Al composition or increasing pair numbers in the SLS stacks. SLS is also less prone to cracks compared to DBR stacks. Superior device performance of blue LED grown on Si(111) substrate with insertion of the $Al_{0.06}Ga_{0.94}N$/GaN SLS cladding underlayer has been reported elsewhere [20]. This section investigates the underlying physical mechanism attributed by the insertion of the $Al_{0.06}Ga_{0.94}N$/GaN SLS cladding underlayer.

4.2.2 Experimental Methods

Samples in this study were grown on 2 inches Si(111) substrates in a commercially available Taiyo Nippon Sanso SR-4000 MOCVD. Trimethylindium [TMIn: $In(CH_3)_3$], trimethylgallium [TMGa: $Ga(CH_3)_3$], trimethylaluminum [TMAl: $Al(CH_3)_3$] and ammonia (NH_3) were used as precursors for In, Ga, Al and N, respectively. Hydrogen (H_2) was used as carrier gas. Monosilane (SiH_4) diluted in hydrogen was used for n-type dopant. The Si(111) substrates were thermally cleaned at 1100°C in H_2 flow prior to the growth. Initially, a 20 nm thin AlN layer was grown at 1100°C on the Si(111) substrates as nucleation layer, followed by 40 pairs of AlN/GaN ML with respective thickness of 5 nm and 20 nm. Subsequently, in the first sample, a

400 nm thick cladding underlayer was grown which consist of 80 pairs of $Al_{0.06}Ga_{0.94}N$/GaN SLS with respective thickness of 2.5 nm for each layer. The $Al_{0.06}Ga_{0.94}N$ portion of the SLS pair was doped with Si ($\sim 1\times10^{18}$ cm^{-3}) to produce a modulation-doped (MD) structure. In the second sample, the SLS cladding underlayer was substituted by a Si-doped ($\sim 1\times10^{18}$ cm^{-3}) GaN layer conventionally used in our LED growth [16-17]. Subsequent layers were kept identical for both samples with 60 nm n-GaN waveguide layer, 10 pairs of 1.5 nm $In_{0.16}Ga_{0.84}N$ wells and 9 nm $In_{0.08}Ga_{0.92}N$:Si barriers in the active layer, and a 10 nm GaN cap layer. Reactor temperature was decreased to 800°C during the active layer growth.

MQW emission peak distribution was evaluated by PL surface mapping with scanning diameter of 48 mm from the wafer center, using a He-Cd laser at excitation wavelength of 325 nm. Emission mechanism was evaluated by temperature-dependent PL method in a pulse tube helium cryostat (Iwatani Mini Cryo) equipped with electrical heater and temperature controller. The MQW was excited by a He-Cd laser with incident beam at perpendicular angle to the sample surface, and emission spectra was collected at perpendicular direction of the surface through monochromator prior detection by charge charge-coupled device (CCD). Structural properties were investigated by cross-sectional TEM observed using JEOL JEM-2010F FasTEM system operating at 200 kV. Standard TEM sample preparation method was used with final thickness of 100 nm. RSM around $(10\bar{1}5)$ diffraction plane was recorded using Philips X'Pert Pro x-ray diffraction system to evaluate stress in the structure.

4.2.3 Results and Discussions

All samples grown in this study are crack-free and show no meltback-etching. Sample with $Al_{0.06}Ga_{0.94}N$/GaN SLS underlayer shows a specular surface for the whole wafer. However, sample with GaN underlayer was cloudy at the wafer edge due to the thick GaN underlayer. PL surface mapping for both samples is shown in Fig. 4.4. MQW emission peak FWHM average for sample with $Al_{0.06}Ga_{0.94}N$/GaN SLS underlayer and GaN underlayer is 25.8 nm and 30.0 nm, respectively, with standard deviation of 2.5% and 11.1%, respectively. The results clearly indicate that $Al_{0.06}Ga_{0.94}N$/GaN SLS underlayer can improve MQW emission wavelength uniformity, and consistent with the author's previous report with a lower MQW pair numbers [20].

Temperature-dependent PL spectra of the samples are shown in Fig. 4.5, with 10 K increment for 10 to 100 K range, and 20 K increment for 100 to 300 K range. Our PL spectra results do not show any yellow-luminescence band, proving that a high quality film has been achieved [21]. The sample with $Al_{0.06}Ga_{0.94}N$/GaN cladding underlayer shows main peak at 3.05 eV (S1) at low temperature. However, the peak at 2.95 eV (S2) grows stronger to become main peak at higher temperatures. The peak at 3.19 eV (B) which is visible at low temperature is from InGaN barrier in the active layer. Meanwhile, the sample with conventional GaN underlayer shows main emission peak at 3.02 (S2) and a small shoulder peak at 3.12 eV (S1). The peak at 3.21 eV (B) is from InGaN barrier in the active layer, which is consistent with the sample with $Al_{0.06}Ga_{0.94}N$/GaN SLS cladding underlayer. Low-energy shoulder peak of the MQW emission in each of the PL spectra is LO phonon replica of peak S2.

A significant intensity drop is observed in both samples when temperature is increased beyond 140 K due to activation of non-radiative recombination centers in the InGaN MQW [22]. An overall red shift of ~65 meV can be seen for MQW peaks in

sample with $Al_{0.06}Ga_{0.94}N$/GaN SLS underlayer compared to that of GaN underlayer. This is due to a stronger QCSE attributed by stronger compressive stress in the MQW influenced by the underlying $Al_{0.06}Ga_{0.94}N$/GaN SLS underlayer [23]. However, the sample with $Al_{0.06}Ga_{0.94}N$/GaN SLS underlayer always demonstrates a higher intensity than that of conventional GaN underlayer because the 1.5 nm thin MQW layer gives minimal effect to electron-hole separation in the MQW.

In order to further understand the emission mechanism in the samples, Gaussian fit was applied to the temperature dependent PL spectra to obtain emission wavelength behavior and integrated intensity of peak energy S2. In an ideal MQW, the PL peak energy should follow Varshni empirical equation [24],

$$E_0(T) = E_0(0) - \alpha T^2/(\beta + T) \tag{4.1}$$

where $E_0(0)$ is the transition energy at 0 K, and α and β are Varshni thermal coefficient constants. Fig. 4.6 shows temperature-dependent of the peak energy S2 in both samples. Solid lines in the figure represent best fit to the Varshni empirical equation, with $E_0(T) = 2.955 - 4.15\times10^{-4}T^2/(836+T)$ for sample with $Al_{0.06}Ga_{0.94}N$/GaN SLS underlayer, and $E_0(T) = 3.021 - 7.16\times10^{-4}T^2/(956+T)$ for sample with GaN underlayer. The Varshni thermal coefficients obtained here are consistent with those obtained from PL and photoreflectance (PR) studies of InGaN film grown on sapphire substrate [25-26]. Our results indicate that the peak S2 in both of the sample is mainly contributed by delocalized excitons at low temperatures until 50 K. Delocalized exciton energy can be estimated by the difference of energy peak position between experimental value and calculated Varshni best fit value at low temperature. The estimated delocalized exciton energy is 4.6 meV in sample with $Al_{0.06}Ga_{0.94}N$/GaN

SLS underlayer, and 7.7 meV in sample with GaN underlayer. Localized excitons give stronger contribution to the MQW emission when the temperature is increased beyond 50 K. With temperature increase, the sample with $Al_{0.06}Ga_{0.94}N$/GaN SLS underlayer shows a smaller emission peak shift than that of conventional GaN underlayer.

Fig. 4.7 shows Arrhenius plot of normalized integrated PL intensity to the function of inverted temperature for emission peak S2 in both samples. In general, the quenching of the luminescence with temperature can be explained by thermal emission of the carriers out of a confining potential with an activation energy correlated with the depth of the confining potential [22]. Activation energies in the InGaN MQW can be obtained by fitting the Arrhenius plot to the equation [27],

$$I(T) = I(0)\left[1 + A_1 \exp\left(-\frac{E_{A1}}{k_B T}\right) + A_2 \exp\left(-\frac{E_{A2}}{k_B T}\right)\right]^{-1} \quad (4.2)$$

where E_{A1} and E_{A2} are activation energies, $I(T)$ is the PL intensity at temperature T, $I_0(0)$ is the PL intensity at absolute zero temperature, and A_1 and A_2 are constants. The solid line in Fig. 4.7 represents best fit to the equation (4.2). The sample with $Al_{0.06}Ga_{0.94}N$/GaN SLS cladding underlayer has activation energy of 10.4 meV and 151.1 meV as shown in Fig. 4.7(a). Meanwhile, the sample with conventional GaN underlayer has activation energy of 8.4 meV and 63.6 meV as shown in Fig. 4.7(b). The fitted activation energy value is consistent with other literatures (e.g., ~35 meV for 450 nm emission InGaN [22], ~6 meV and ~43 meV for 380 nm emission InGaN MQW [25], ~63 meV for 370 nm emission InGaN [28], and ~16 meV and ~171 meV for 477 nm emission InGaN) [29]. The lower activation energy (E_{A1}) in each sample (10.4 meV and 8.4 meV) is completely attributed by non-radiative recombination centers in the InGaN MQW [22,25]. The activation energy of 63.6 meV in sample with conventional

GaN underlayer is attributed by the thermal barrier to escape from localized states and/or to capture at non-radiative recombination centers in the InGaN wells, since the activation energy is smaller than the band offset and band-gap energy difference between the wells and the barriers [22,26,28]. However, the large activation energy of 151.1 meV in sample with $Al_{0.06}Ga_{0.94}N$/GaN SLS cladding underlayer suggest that thermal quenching in that sample is attributed by thermal escape of electrons and/or holes from the InGaN wells into the InGaN barriers [29].

The value of η_{iqe} can be estimated from integrated PL intensity ratio of 300 K to 10 K $(I_{300\,K}/I_{10\,K})$, assuming that η_{iqe} at 10 K is 100%. The estimated η_{iqe} in sample with $Al_{0.06}Ga_{0.94}N$/GaN underlayer and sample with GaN underlayer is 29.4% and 20.6%, respectively. The estimation is consistent with our earlier report with a lower quantity of MQW pair [30]. The higher η_{iqe} in sample with $Al_{0.06}Ga_{0.94}N$/GaN SLS underlayer agrees well with mechanism of thermal quenching in InGaN MQW discussed earlier.

Structural analysis is important to understand the mechanism of activation energy difference with the modification of underlayer. TEM study on $[1\bar{1}00]$ cross-section of GaN was observed to investigate dislocation characteristics. TEM dark-field (DF) images of the sample with $Al_{0.06}Ga_{0.94}N$/GaN underlayer are shown in Fig. 4.8, with $\boldsymbol{g}=[0002]$ and $\boldsymbol{g}=[11\bar{2}0]$ diffraction conditions. Screw dislocations with $\boldsymbol{b}=[0001]$ and edge dislocations with $\boldsymbol{b}=(1/3)[11\bar{2}0]$ are visible as white lines in respective diffraction plane. Mixed dislocation with $\boldsymbol{b}=(1/3)[11\bar{2}3]$ can be observed in both planes, according to the $\boldsymbol{g}\times\boldsymbol{b}$ invisibility criterion.

In normal GaN underlayer, TDs from AlN/GaN ML propagate vertically through the layer to the surface (not shown) [30,33]. In the sample with

$Al_{0.06}Ga_{0.94}N$/GaN SLS cladding underlayer, TDs surpassing the interface between AlN/GaN ML and $Al_{0.06}Ga_{0.94}N$/GaN SLS bend at abrupt angle and radically disappear by creating dislocation close-loop in the $Al_{0.06}Ga_{0.94}N$/GaN SLS cladding layer, as marked by white arrows in the figures. Edge type of dislocations can be seen inclined towards $<1\bar{1}00>$ direction before annihilation as pointed out by white arrows in the Fig. 4.8(b) [31]. The $Al_{0.06}Ga_{0.94}N$/GaN SLS is more effective to block screw type of dislocations than that of edge type of dislocations as penetration of most of the screw dislocation lines are blocked at the ML/SLS interface and lower region of the SLS layer, compared to that of edge dislocations which exceeds into the middle and upper region of the SLS layer before inclination. TDD along the upper edge of the $Al_{0.06}Ga_{0.94}N$/GaN SLS cladding layer is estimated to be 3.4×10^{9} cm^{-2} for screw and mixed component of TDs under $\boldsymbol{g}=(0002)$ diffraction condition, and 6.5×10^{9} cm^{-2} for edge and mixed component of TDs under $\boldsymbol{g}=(11\bar{2}0)$ diffraction condition. The $Al_{0.06}Ga_{0.94}N$/GaN SLS underlayer shows approximately one order magnitude lower TDD than that of conventional growth method on Si(111) substrate obtained by TEM [30,33].

Further understanding on the effect of $Al_{0.06}Ga_{0.94}N$/GaN SLS cladding underlayer to the structural properties of the samples can be derived from RSM. Fig. 4.9 shows RSM of sample grown with $Al_{0.06}Ga_{0.94}N$/GaN SLS underlayer in (a) and GaN underlayer in (b), recorded around $(10\bar{1}5)$ reflection. A contour of intensity observed in the sample with $Al_{0.06}Ga_{0.94}N$/GaN SLS underlayer is associated with fringes from the thin SLS periods. In-plane lattice constant of GaN-based film can be calculated using the equation,

$$a_{(10\bar{1}5)} = \frac{2}{\sqrt{3}Q_x} \tag{4.3}$$

where Q_x is the deviation vector component at horizontal direction [32]. From Fig. 4.9, the measured in-plane lattice constant for GaN in sample with $Al_{0.06}Ga_{0.94}N$/GaN SLS underlayer is 3.1698 Å. The obtained value is consistent with in-plane GaN lattice constant obtained from a control sample grown until $Al_{0.06}Ga_{0.94}N$/GaN SLS cladding underlayer (without waveguide, active and capping layer). In-plane lattice constant for GaN in sample with GaN underlayer is 3.1758 Å. The in-plane lattice constant clearly indicates that a larger compressive strain exist in GaN layer in sample with $Al_{0.06}Ga_{0.94}N$/GaN SLS underlayer relative to that of sample with conventional GaN underlayer. The compressive strain in GaN layer of the $Al_{0.06}Ga_{0.94}N$/GaN pair is suggested to force TD lines in the sample to bend abruptly, thus reducing TDD in the upper region of the sample. The lower TDD subsequently reduces non-radiative recombination centers in the InGaN MQW and simultaneously increases η_{iqe} of the InGaN MQW.

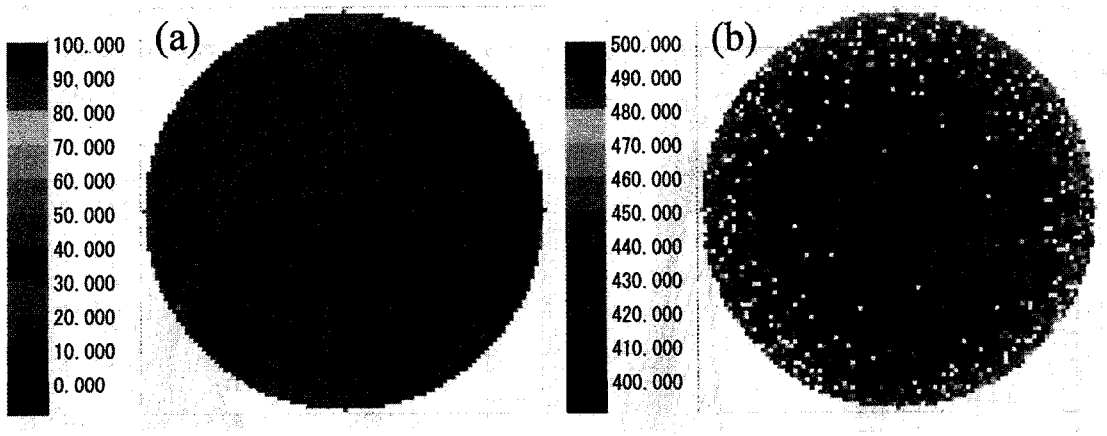

Fig. 4.4. PL surface mapping showing emission peak wavelength full-width at half-maximum (FWHM) distribution for wafer with $Al_{0.06}Ga_{0.94}N$/GaN SLS cladding underlayer in (a) and with GaN underlayer in (b).

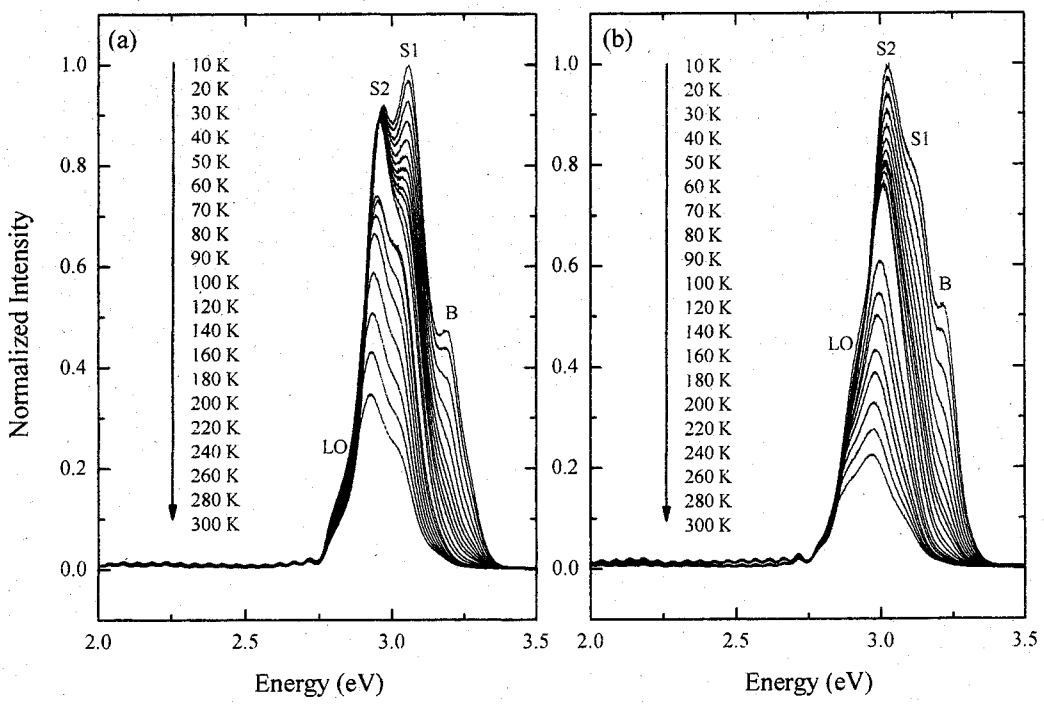

Fig. 4.5. PL spectra of (a) sample with $Al_{0.06}Ga_{0.94}N$/GaN SLS underlayer and (b) sample with GaN underlayer recorded in 10 K to 300 K temperature range.

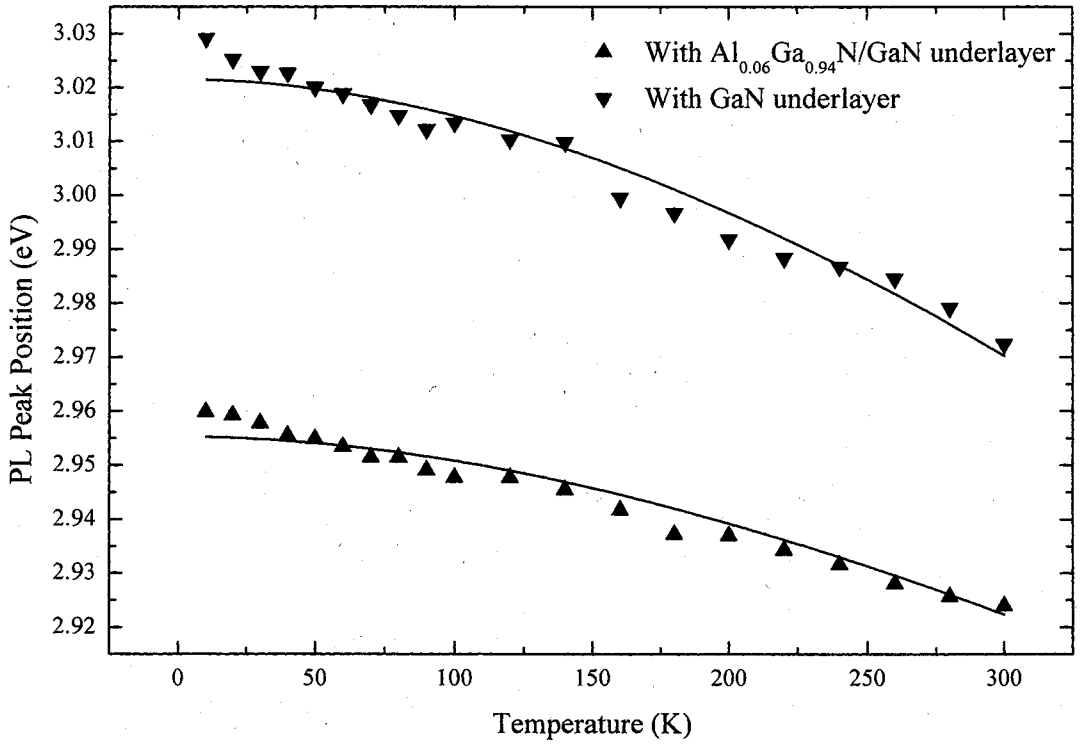

Fig. 4.6. Temperature-dependent of the peak energy S2 in sample with $Al_{0.06}Ga_{0.94}N$/GaN underlayer and GaN underlayer.

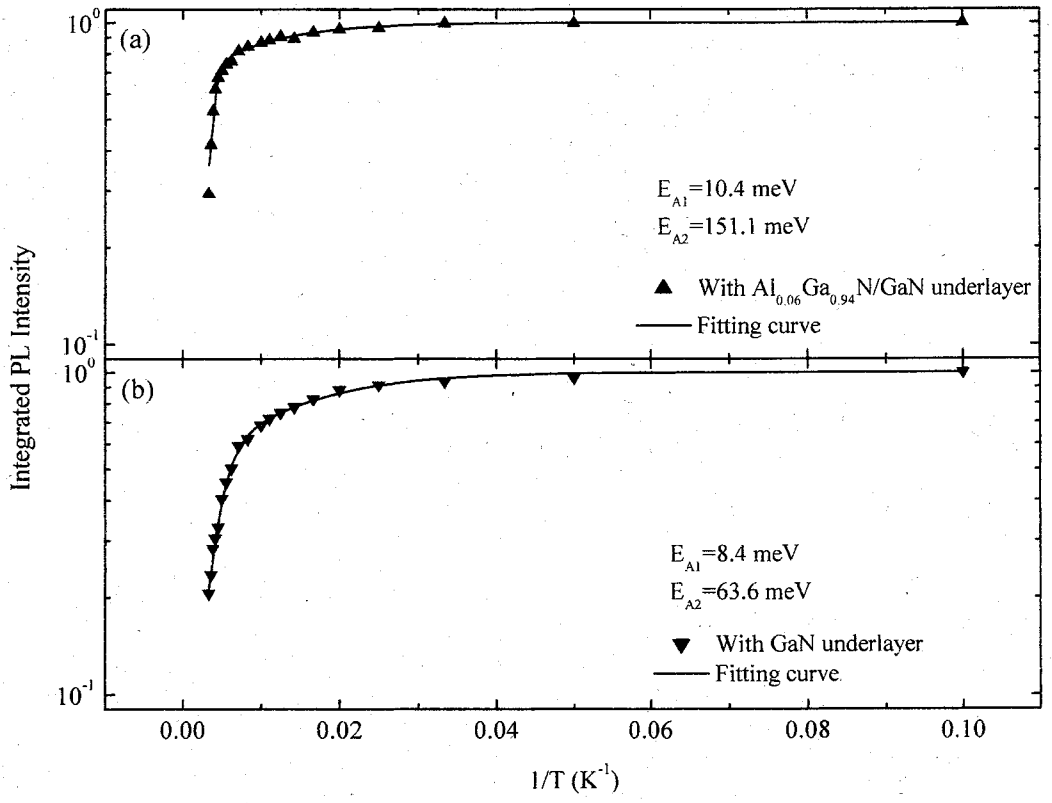

Fig. 4.7. Arrhenius plot of normalized integrated intensity to the function of inverted temperature for (a) sample with $Al_{0.06}Ga_{0.94}N$/GaN SLS underlayer and (b) sample with GaN underlayer. Experimental results are presented by triangle marks, and the solid lines are their fitting curve according to equation (4.2).

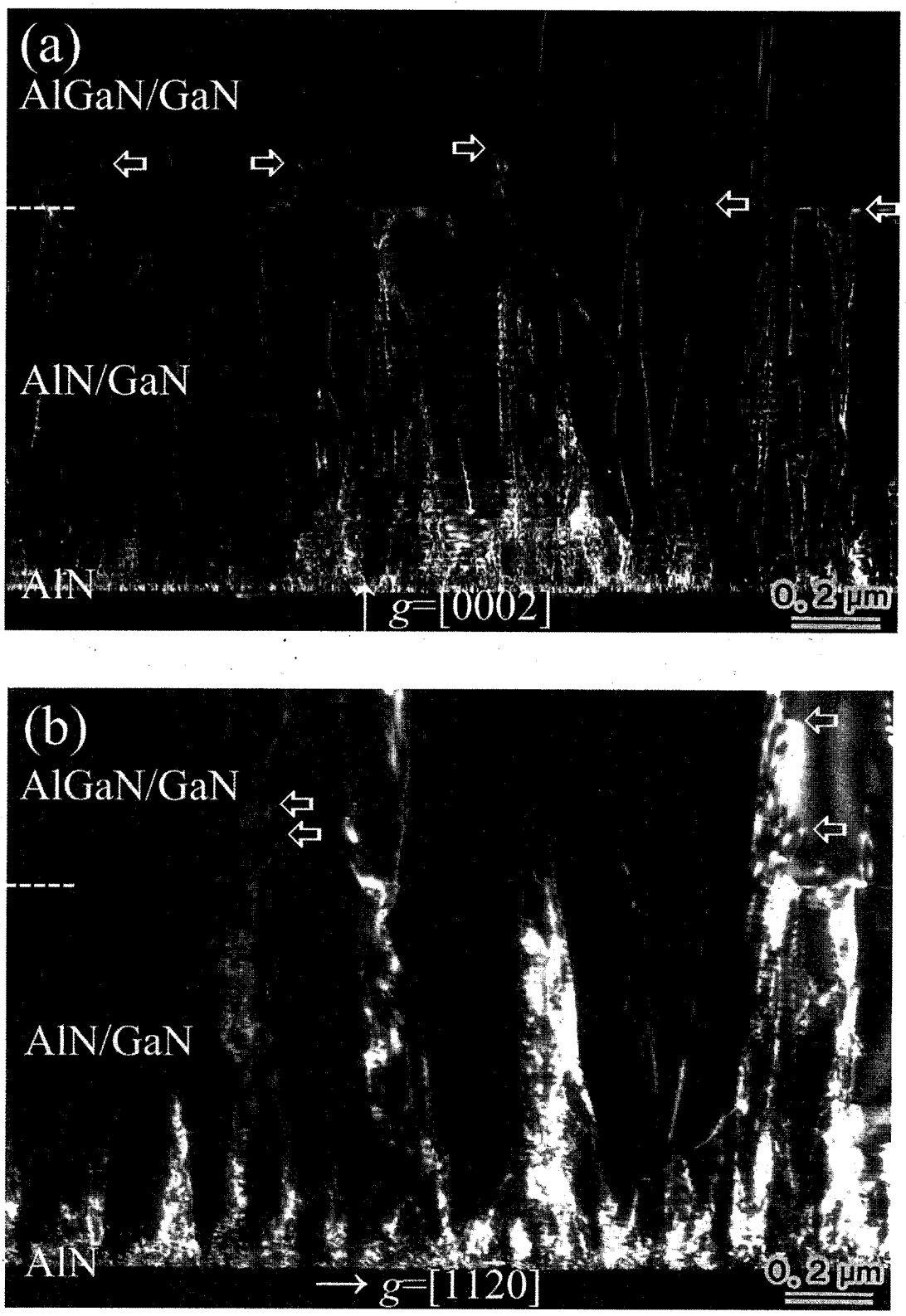

Fig. 4.8. TEM DF image of sample with $Al_{0.06}Ga_{0.94}N$/GaN SLS cladding underlayer. Diffraction plane is marked in the image.

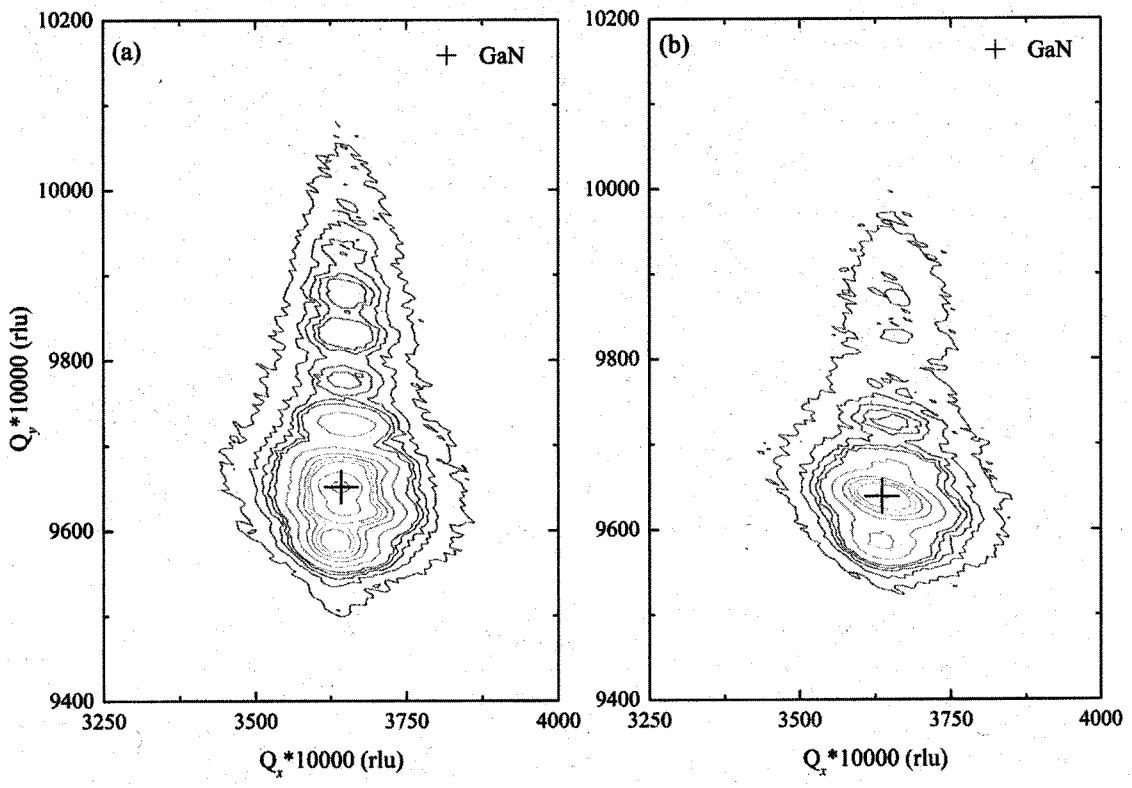

Fig. 4.9. RSM around $(10\bar{1}5)$ diffraction plane of (a) sample with $Al_{0.06}Ga_{0.94}N$/GaN underlayer and (b) sample with GaN underlayer. GaN position is marked in each figure.

4.3 Growth of InGaN-based Laser Diode Structure on Silicon (111) Substrate

4.3.1 Introduction

GaN and its tertiary and quaternary alloys are very promising materials for light-emitting optoelectronic devices such as LED and LD, with emission range from deep ultra-violet (DUV) to infra-red (IR) region. GaN growth for light-emitting devices such as LED and LD has been performed on sapphire, SiC and GaN free-standing substrates. On the other hand, Si is also a promising substrate for GaN growth, which offers many advantages such as low cost, large diameter, good thermal conductivity for high-power devices, vertical electrode capability and the possibility for integration with Si-based electronics to create a monolithic optical and electronics integrated circuit (OEIC).

Despite of its large thermal and lattice mismatch with GaN, several groups have reported good quality GaN epitaxial growth and devices on Si(111) substrate [1-6]. However, growth of GaN on Si is more focused for LED [2-5] and HEMT [10]. On the other hand, growth for GaN-based LD is performed on sapphire [34-36], SiC [37-38] and GaN free-standing [39-40] substrates. In the author's knowledge, successful growth of GaN-based LD structure on Si substrate for current pumping has never been reported, due to the complexity during layer growth and necessity for thick structure, which may result to cracks in the epitaxial layer. AlN is widely used as buffer layer for GaN growth on Si. Several reports use thick AlN buffer layer to prevent the formation of meltback-etching and cracks [2,41]. However, thickening the AlN buffer layer will produce higher series resistance in the final device due to the insulating nature of AlN,

which is not practical for LD with vertical electrode. This study reports the growth and material characterization of LD structures on Si(111) substrate by utilizing thin AlN buffer layer and AlN/GaN ML intermediate layer. A standard LD structure on GaN(0001) free-standing substrate is also prepared for comparison.

4.3.2 Experimental Methods

The growth of LD structures in this report was carried out in a commercially available MOCVD with horizontal reactor system. Trimethylgallium (TMGa), trimethylindium (TMIn), trimethylaluminum (TMAl) and ammonia (NH_3) were used as source materials, and hydrogen (H_2) was used as the carrier gas. Two type of LD structures grown on Si(111) substrate, denoted as sample A and sample B, and one LD structure grown on GaN free-standing substrate, denoted as sample C were prepared for comparison. In this study, sample C is a standard LD structure, and the growth for sample A and B is optimized to reach or exceed the performance of the standard sample.

Prior to the growth of both LD structures on Si(111) substrate, a thin high-temperature AlN buffer layer and AlN/GaN ML intermediate layer were grown to improve the structural and optical quality of the subsequent layers [1-5]. Sample A consists of a 500 nm thick n-AlGaN cladding layer, n-GaN waveguide layer, active layer with 3 periods of MQW consisting of 4 nm thick undoped $In_{0.10}Ga_{0.90}N$ wells and 8.0 nm thick Si-doped $In_{0.03}Ga_{0.97}N$ barriers, GaN waveguide layer, p-AlGaN electron-block layer, 500 nm thick p-AlGaN cladding layer and p-GaN contact layer. Sample B consists of almost identical structure with sample A, except n- and p-type cladding layers which were replaced with n- and p-type $Al_{0.06}Ga_{0.94}N$/GaN SLS layers. SLS layers are generally used to reduce TDD in the active layer [36,42] and to enhance

carrier concentration in the cladding layer [42,44]. In sample C, a thick n-GaN was used as buffer layer prior to the growth of LD layers. All subsequent layers in this sample are identical to sample A. Full structure for each sample is shown in Fig. 4.10.

Surface morphology of the samples was characterized using atomic force microscopy (AFM). Crystal quality and structural property were characterized by HRXRD. Temperature-dependent PL measurement from 10 to 300 K was performed using a He-Cd laser at 325 nm emission line as excitation source to characterize the MQW performance. Emission from the MQW was collected using CCD positioned normal to the sample surface. The MQW indium composition x was estimated from PL peak energy at 300 K on sample C using the relation, $E_g(x)=3.412(1-x)+0.65x-2.6x(1-x)$ eV, where E_g is 3.412 eV for GaN [47] and 0.65 eV for InN [48]. E_g is the effective excitonic band gap energy and the value -2.6 is the bowing parameter for strained c-plane $In_xGa_{1-x}N$ layer on GaN for $0<x<0.2$ [43,49]. The MQW layer thickness was determined by software simulation based on HRXRD ω-2θ characterization and scanning transmission electron microscopy (STEM) cross-sectional image.

4.3.3 Results and Discussions

Specular and meltback-etching free surfaces have been achieved for all samples in our study. AFM, HRXRD and PL properties of sample A, B and C are summarized in Table IV.II. STEM cross-sectional image of sample A and B are shown in Fig. 4.11. The images clearly show that an abrupt layer interface has been grown in both of the structures, including the MQW. The images also indicate that an identical thickness of wells and barriers has been grown in both of the samples. AFM surface morphology image in Fig. 4.12 shows that terraces can be clearly observed in samples grown on Si

substrate. Screw component of dislocations and pure edge dislocations are clearly visible in the samples [36,45]. In contrast, the sample grown on GaN substrate shows straight steps [45]. The RMS roughness measured on 3×3 μm area is 0.44 nm and 0.48 nm for sample A and B, respectively, while the peak to valley (P-V) is 3.58 nm and 3.59 nm for sample A and B, respectively. Despite a slight increase of roughness and P-V value for sample B compared to sample A, these values are more than 3 times larger than the structure on GaN substrate indicated by sample C.

Fig. 4.13 shows the HRXRD GaN (0004) ω-2θ scan for sample A, B and C. The result shows strong $In_{0.10}Ga_{0.90}N/In_{0.03}Ga_{0.97}N$ MQW fringes of 0^{th}, -1^{st}, -2^{nd} and -3^{rd} orders in all samples. The $+1^{st}$ and $+2^{nd}$ orders of the fringes, however, are weak in all samples. Note that the $+1^{st}$ and $+2^{nd}$ order fringes of the MQW in samples grown on Si(111) overlap with fringes from AlN/GaN ML, resulting a higher intensity fringes at 36.7 deg. and 37.2 deg. relative to other AlN/GaN ML fringes. The MQW mean period thickness is 12.1±0.3 nm, 12.4±0.3 nm, and 11.8±0.3 nm for sample A, B and C, respectively. The higher-order fringes indicate that a good quality MQW layer with abrupt interfaces has been achieved in all of the samples. The consistent thickness in all samples indicates that MQW growth on Si substrate does not show any enormous change in the period thickness compared to growth on GaN substrate.

PL characteristics at 10 K and 300 K for sample A, B and C is shown in Fig. 4.14. The band-to-band photon energy emitted from the $In_{0.10}Ga_{0.90}N/In_{0.03}Ga_{0.97}N$ MQW in the LD structures measured at 10 K is 2.84 eV, 2.88 eV and 2.89 eV for sample A, B and C, respectively. The strong peaks at ~3.06 eV, ~3.16 eV and ~3.24 eV are from Mg-dopant in the 500 nm thick p-type cladding layer and contact layer in the samples. The appearance of MQW fringes modulated by Fabry-Perot interference at

~2.7 eV confirms that a smooth and abrupt layer interfaces has been achieved in our samples. Measurements at 300 K reveals a small red-shift in all of the samples, with MQW band-to-band photon energy of 2.81 eV, 2.86 eV and 2.88 eV in sample A, B and C, respectively. Note than wider FWHM in sample C at 300 K is attributed by the combination of lower-energy fringe peaks (~2.8 eV) into the main peak, which is commonly seen in very high quality interfacial layer.

Light emission intensity ratio from the samples at 10 K is 93, 33 and 100 for sample A, B and C, respectively. The lower emission intensity in sample B is suggested to be attributed by higher reflectivity of the AlGaN/GaN SLS p-type cladding layer which limits He-Ne laser light from reaching the MQW, and limits the extraction of photon from active layer region. Interestingly, sample B shows smaller photon emission intensity difference when the temperature is increased to 300 K, when compared to that of sample A.

In order to investigate the peak behavior of the MQW, the MQW peak from temperature-dependent PL measurement is plotted in Fig. 4.15, with 10 K interval for temperature from 10 to 100 K, and 20 K interval for the next temperature increment until 300 K. A clear "S-shaped" peak behavior can be observed in all samples. The MQW emission peak red-shifts when the temperature is increased from 10 to 70 K, blue-shifts when the temperature is increased from 70 to 120-140 K, and returns to red-shifts when the temperature is increased from 120-140 to 300 K. This result is consistent with report by Cho *et al.* [46]. However, with the increase of temperature, a stronger red-shift trend is observed in both samples grown on Si(111) substrate compared to that of GaN(0001) substrate. This trend is believed to be influenced by QCSE, due to existence of strong tensile stress for GaN structure grown on Si(111)

substrate [6]. Larger QCSE can be confirmed in Sample A, as the whole emission peak was red-shifted, compared to that of sample B and C.

Gaussian fitting has been performed to the temperature-dependent PL using a software called Origin to obtain the MQW normalized integrated intensity, as shown in Fig. 4.16. Assuming that the η_{iqe} of the samples at 10 K is 100%, the η_{iqe} at 300 K is estimated to be 0.06%, 0.34% and 1.21% for sample A, B and C, respectively. The Sample B shows one order of magnitude higher η_{iqe} than that of sample A, probably due to lower QCSE in the MQW produced by the SLS cladding layer. The η_{iqe} values in this study are generally low due to the thick p-type cladding layer above the active layer in the LD structure. The significant decrease of luminescence at ~70 K until ~180-200 K in our normalized integrated intensity result can be speculated by the activation of non-radiative process which dominates the carrier-recombination at this temperature [46]. The temperature-dependent peak behavior and temperature-dependent normalized integrated intensity reveal that $Al_{0.06}Ga_{0.94}N$/GaN SLS layer is effective to reduce QCSE and improve η_{iqe} in InGaN-based MQW grown on Si(111) substrate.

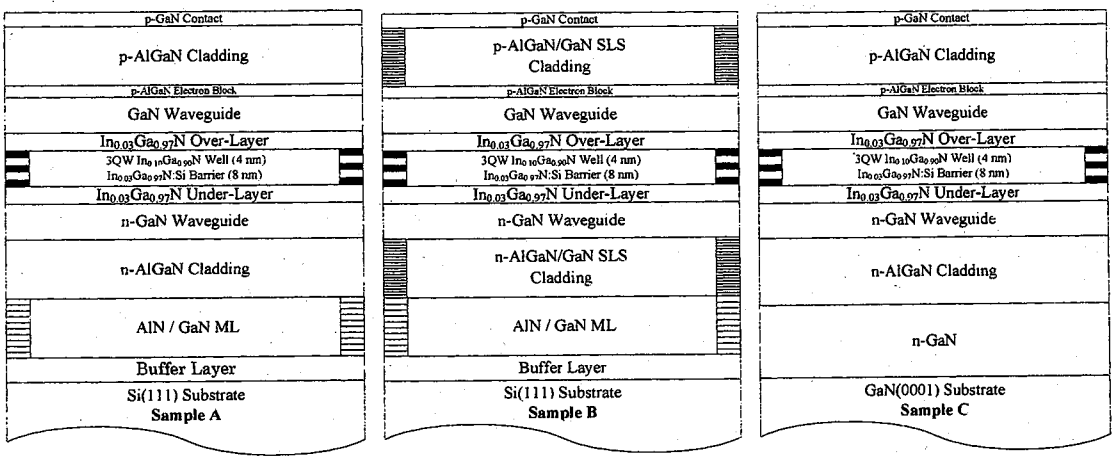

Fig. 4.10. Layer structure for sample A (left), B (center) and C (right).

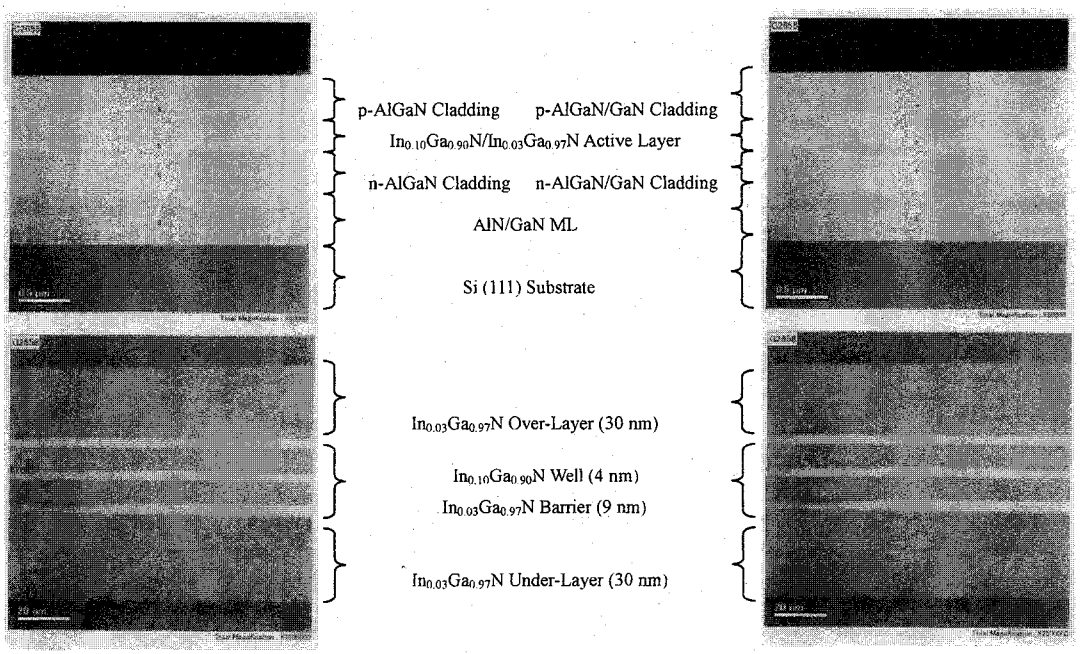

Fig. 4.11. STEM cross-sectional image of sample A (left) and B (right). Images in the upper row show the entire epitaxial layer. The lower row shows focused image at active layer region in each respective sample.

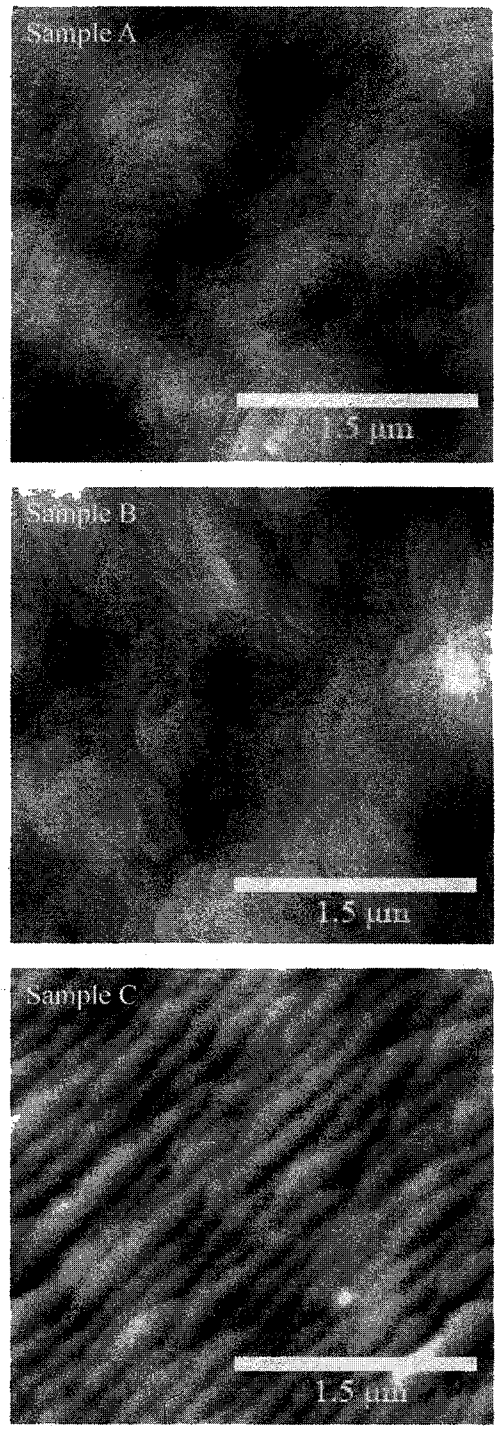

Fig. 4.12. AFM images of the sample surface in 3×3 μm area.

Table IV.II. Sample properties from each characterization method.

Characterization Method		**Sample A**	**Sample B**	**Sample C**
AFM	RMS (nm)	0.44	0.48	0.14
3×3 μm	P-V (nm)	3.58	3.59	1.13
PL at 10 K	Intensity (a. u.)	93	33	100
	MQW Peak (eV)	2.84	2.88	2.89
	FWHM (meV)	173.3	~139.7 (at 0.6)	106.4
at 300 K	MQW Peak (eV)	2.81	2.86	2.88
	FWHM (meV)	93.5	97.2	196.6

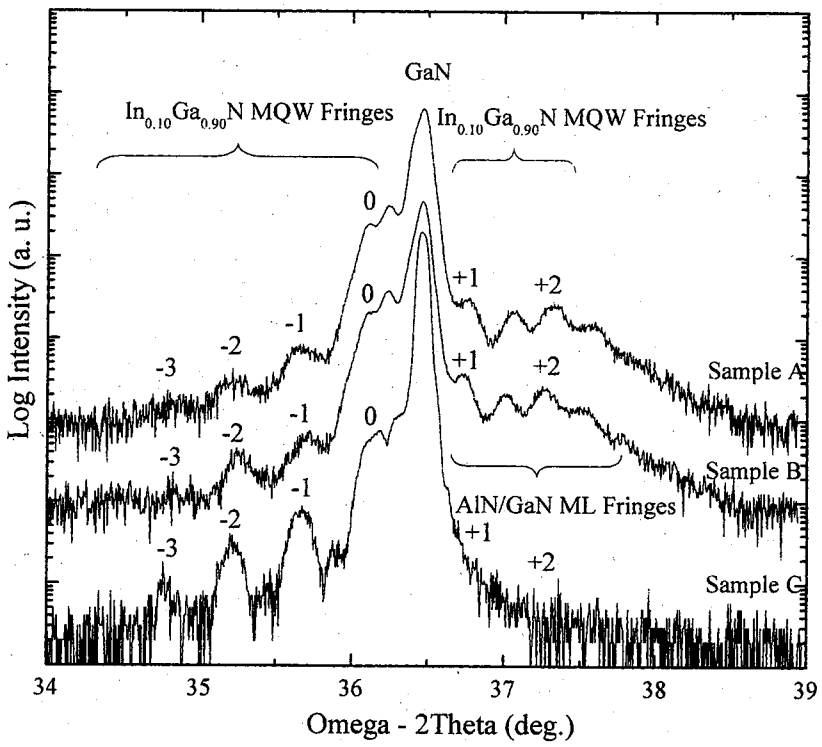

Fig. 4.13. HRXRD GaN (0004) ω-2θ scan for sample A, B and C.

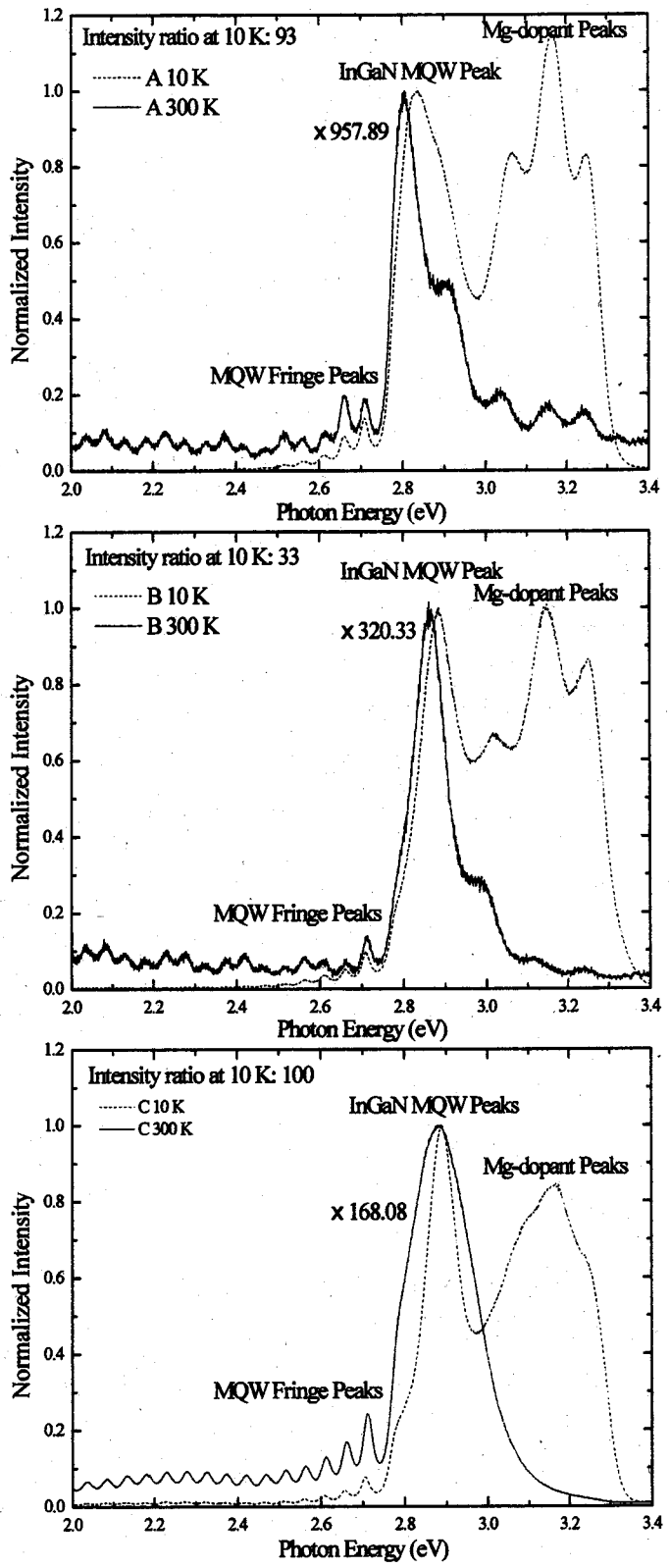

Fig. 4.14. PL characteristics at 10 and 300 K for sample A (left), B (center) and C (right).

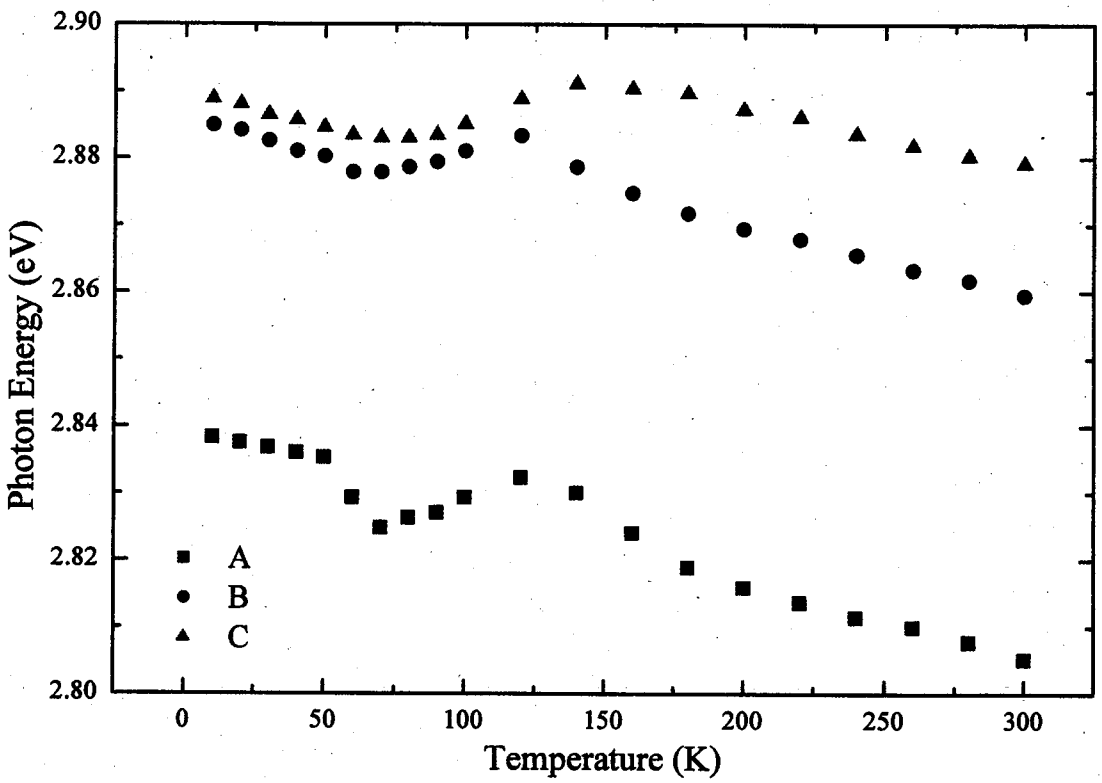

Fig. 4.15. Temperature-dependent MQW peak behavior.

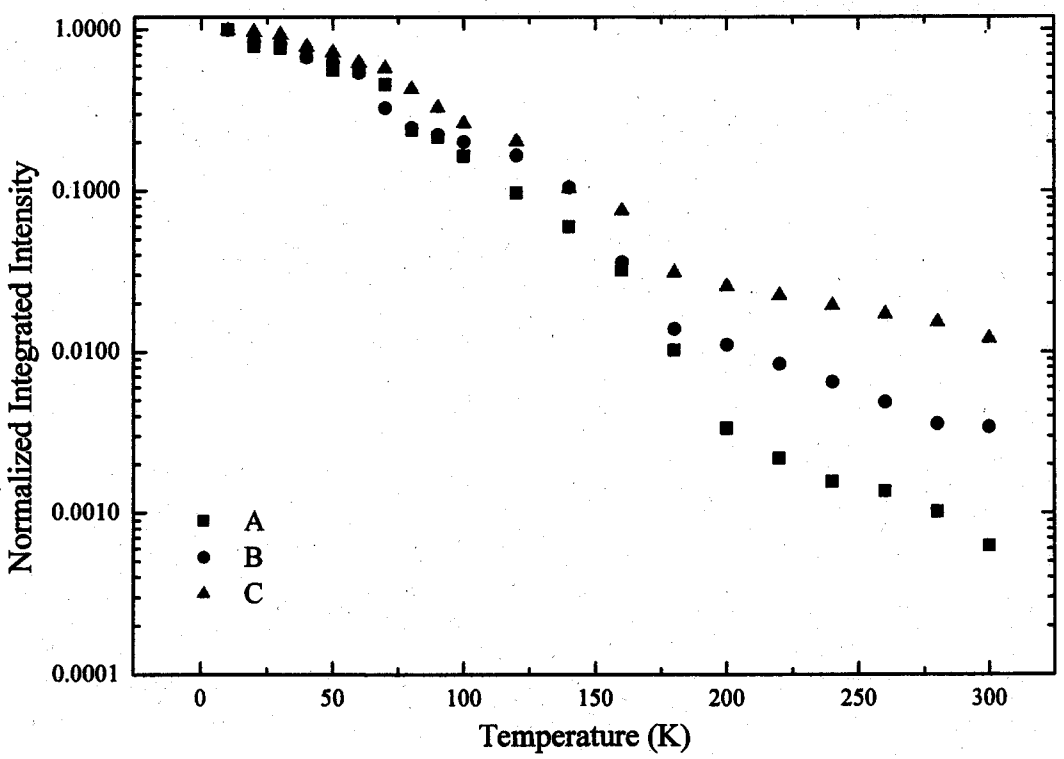

Fig. 4.16. Temperature-dependent normalized integrated intensity.

4.4 Conclusions

In section 4.1, we report reduction of TD for GaN-based epitaxy grown on Si(111) by $Al_{0.06}Ga_{0.94}N$/GaN SLS cladding underlayer, relative to $Al_{0.03}Ga_{0.97}N$ bulk cladding underlayer. TEM bright-field images confirm that the SLS cladding layer efficiently suppresses TD from propagating into subsequently grown layer. A relatively high η_{iqe} of 31.6% has been achieved in sample with the underlying SLS cladding layer, when MQW thickness is optimized to 2 nm.

A detailed study of emission mechanism and strain effect of the $Al_{0.06}Ga_{0.94}N$/GaN SLS cladding underlayer is reported in section 4.2. Compressive strain in GaN layer portion of the $Al_{0.06}Ga_{0.94}N$/GaN SLS pair forces threading dislocation lines to bend abruptly, thus reduces TD penetration into the upper layer in the structure and subsequently increases η_{iqe} of MQW in the particular sample. Moreover, the underlayer also improves InGaN emission peak wavelength uniformity and FWHM compared to that of conventional GaN underlayer.

In section 4.3, good quality $In_{0.10}Ga_{0.90}N/In_{0.03}Ga_{0.97}N$ LD structures were successfully grown on Si(111) substrate, using thin high-temperature AlN buffer layer and AlN/GaN ML intermediate layers. The samples grown on Si(111) substrate in this study are mirror-like and free from meltback-etching. Our results reveal that the replacement of AlGaN bulk layer with SLS layer consisted of $Al_{0.06}Ga_{0.94}N$/GaN into the n- and p-type cladding layer could improve MQW properties, and increase η_{iqe} of the sample.

References

[1] H. Ishikawa, G. Y. Zhao, N. Nakada, T. Egawa, T. Jimbo and M. Umeno, Jpn. J. Appl. Phys. **38**, L492 (1999).

[2] T. Egawa, B. Zhang, N. Nishikawa, H. Ishikawa, T. Jimbo and M. Umeno, J. Appl. Phys. **91**, 528 (2002).

[3] T. Egawa, T. Moku, H. Ishikawa, K. Ohtsuka and T. Jimbo, Jpn. J. Appl. Phys. **41**, L663 (2002).

[4] T. Egawa, B. Zhang and H. Ishikawa, IEEE Elect. Dev. Lett. **26**, 169 (2005).

[5] B. Zhang, T. Egawa, H. Ishikawa, Y. Liu and T. Jimbo, Jpn. J. Appl. Phys. **42**, L226 (2003).

[6] A. Dadgar, J. Christen, T. Riemann, S. Richter, J. Bläsing, A. Diez, A. Krost, A. Alam and M. Heuken, Appl. Phys. Lett. **78**, 2211 (2001).

[7] A. Dadgar, C. Hums, A. Diez, J. Bläsing and A. Krost, J. Cryst. Growth **297**, 279 (2006).

[8] K. Cheng, M. Leys, S. Degroote, M. Germain and G. Borghs, Appl. Phys. Lett. **92**, 192111 (2008).

[9] K. Y. Zang, Y. D. Wang, L. S. Wang, S. Y. Chow and S. J. Chua, J. Appl. Phys. **101**, 093502 (2007).

[10] S. L. Selvaraj, T. Ito, Y. Terada and T. Egawa, Appl. Phys. Lett. **90**, 173506 (2007).

[11] J. K. Son, S. N. Lee, T. Sakong, H. S. Paek, O. Nam, Y. Park, J. S. Hwang, J. Y. Kim and Y. H. Cho, J. Cryst. Growth **287**, 558 (2006).

[12] S. F. Chichibu, A. Shikanai, T. Deguchi, A. Setoguchi, R. Nakai, E. Nakanishi, K. Wada, S. P. DenBaars, T. Sota and S. Nakamura, Jpn. J. Appl. Phys. **39**, 2417 (2000).

[13] Y. H. Cho, G. H. Gainer, A. J. Fischer, J. J. Song, S. Keller, U. K. Mishra and S. P. DenBaars, Appl. Phys. Lett. **73**, 1370 (1998).

[14] T. Egawa, B. Zhang, N. Nishikawa, H. Ishikawa, T. Jimbo and M. Umeno, J. Appl. Phys. **91**, 528 (2002).

[15] H. Ishikawa,.K. Asano, B. Zhang, T. Egawa and T. Jimbo, Phys. Stat. Sol. A **201**, 2653 (2004).

[16] T. Egawa, B. Zhang and H. Ishikawa, IEEE Elect. Dev. Lett. **26**, 169 (2005).

[17] B. Zhang, T. Egawa, H. Ishikawa, Y. Liu and T. Jimbo, Jpn. J. Appl. Phys. **42**, L226 (2003).

[18] A. Dadgar, J. Bläsing, A. Diez, A. Alam, M. Heuken and A. Krost, Jpn. J. Appl. Phys. **39**, L1183 (2000).

[19] T. Riemann, T. Hempel, J. Christen, P. Veit, R. Clos, A. Dadgar, A. Krost, U. Haboeck and A. Hoffman, J. Appl. Phys. **99**, 123518 (2006).

[20] B. A. B. Ahmad Shuhaimi, P. C. Khai, T. Suzue, Y. Nomura and T. Egawa, Mater. Res. Soc. Symp. Proc. **1167**, O04-01 (2009).

[21] M. A. Reshchikov and H. Morkoç, J. Appl. Phys. **97**, 061301 (2005).

[22] Y. H. Cho, G. H. Gainer, A. J. Fischer, J. J. Song, S. Keller, U. K. Mishra and S. P. DenBaars, Appl. Phys. Lett. **73**, 1370 (1998).

[23] S. Chichibu, T. Sota, K. Wada and S. Nakamura, J. Vac. Sci. Technol. B **16**, 2204 (1998).

[24] Y. P. Varshni, Physica **34**, 149 (1967).

[25] M. Hao, J. Zhang, X. H. Zhang and S. Chua, Appl. Phys. Lett. **81**, 5129 (2002).

[26] W. Shan, B. D. Little, J. J. Song, Z. C. Feng, M. Schurman and R. A. Stall, Appl. Phys. Lett. **69**, 3315 (1996).

[27]P. J. Dean, Phys. Rev. **157**, 655 (1967).

[28]K. L. Teo, J. S. Colton, P. Y. Yu, E. R Weber, M. F. Li, W. Liu, K. Uchida, H. Tokunaga, N. Akutsu and K. Matsumoto, Appl. Phys. Lett. **73**, 1697 (1998).

[29]Y. Sun, Y. H. Cho, H. M. Kim and T. W. Kang, Appl. Phys. Lett. **87**, 093115 (2005).

[30]B. A. B. Ahmad Shuhaimi, T. Suzue, Y. Nomura, Y. Maki and T. Egawa, Mater. Res. Soc. Symp. Proc. **1167**, O02-05 (2009).

[31]N. Kuwano, Y. Kugiyama, Y. Nishikouri, T. Sato and A. Usui, J. Cryst. Growth **311**, 3085 (2009).

[32]D. K. Bowen and B. K. Tanner, *High Resolution X-ray Diffraction and Topography*, CRC Press, United States of America, p. 157 (1998).

[33]H. Lahrèche, P. Vennéguès, O. Tottereau, M. Laügt, P. Lorenzini, M. Leroux, B. Beaumont and P. Gibart, J. Cryst. Growth **217**, 13 (2000).

[34]S. Nakamura, M. Senoh, S. Nagahama, N. Iwasa, T. Yamada, T. Matsushita, Y. Sugimoto and H. Kiyoku, Appl. Phys. Lett. **69**, 1477 (1996).

[35]S. Nakamura, M. Senoh, S. Nagahama, N. Iwasa, T. Yamada, T. Matsushita, Y. Sugimoto and H. Kiyoku, Appl. Phys. Lett. **69**, 3034 (1996).

[36]S. Nakamura, M. Senoh, S. Nagahama, N. Iwasa, T. Yamada, T. Matsushita, H. Kiyoku, Y. Sugimoto, T. Kozaki, H. Umemoto, M. Sano and K. Chocho, Appl. Phys. Lett. **72**, 211 (1998).

[37]A. Kuramata, S. Kubota, R. Soejima, K. Domen, K. Horino, P. Hacke and T. Tanahashi, Jpn. J. Appl. Phys. **38**, L481 (1999).

[38]J. Edmond, A. Abare, M. Bergman, J. Bharathan, K. L. Bunker, D. Emerson, K. Haberern, J. Ibbetson, M. Leung, P. Russel and D. Slater, J. Cryst. Growth **272**, 242 (2004).

[39]M. Kuramoto, C. Sasaoka, Y. Hisanaga, A. Kimura, A. Yamaguchi, H. Sunakawa, N. Kuroda, M. Nido, A. Usui and M. Mizuta, Jpn. J. Appl. Phys. **38**, L184 (1999).

[40]S. Nakamura, M. Senoh, S. Nagahama, N. Iwasa, T. Yamada, T. Matsushita, H. Kiyoku, Y. Sugimoto, T. Kozaki, H. Umemoto, M. Sano and K. Chocho, Jpn. J. Appl. Phys. **37**, L309 (1998).

[41]D. K. Kim, Solid-State Electronics **51**, 1005 (2007).

[42]M. Shiori, M. Čeh, S. Šturm, C. C. Chuo, J. T. Hsu, J. R. Yang and H. Saijo, J. Appl. Phys. **100**, 013110 (2006).

[43]M. Kubota, K. Okamoto, T. Tanaka and H. Ohta, Appl. Phys. Lett. **92**, 011920 (2008).

[44]K. Kumakura, T. Makimoto and N. Kobayashi, Jpn. J. Appl. Phys Part 1 **39**, 2428 (2000).

[45]B. Heying, E. J. Tarsa, C. R. Elsass, P. Fini, S. P. DenBaars and J. S. Speck, J. Appl. Phys. **85**, 6470 (1999).

[46]Y. H. Cho, G. H. Gainer, A. J. Fischer, J. J. Song, S. Keller, U. K. Mishra and S. P. DenBaars, Appl. Phys. Lett. **73b**, 1370 (1998).

[47]S. F. Chichibu, K. Torii, T. Deguchi, T. Sota, A. Setoguchi, H. Nakanishi, T. Azuhata and S. Nakamura, Appl. Phys. Lett. **76**, 1576 (2000).

[48]T. Inushima, V. V. Mamutin, V. A. Vekshin, S. V. Ivanov, T. Sakon, M. Motokawa and S. Ohoya, J. Cryst. Growth **227-228**, 481 (2001).

[49]C. Wetzel, T. Takeuchi, S. Yamaguchi, H. Katoh, H. Amano and I. Akasaki, Appl. Phys. Lett. **73**, 1994 (1998).